The Fate of Saharan Dust Across the Atlantic and Implications for a Central American Dust Barrier

E. Nowottnick[1], P. Colarco[2], A. da Silva[3], D. Hlavka[4], M. McGill[4]

[1]Atmospheric and Oceanic Sciences, University of Maryland, College Park, MD, USA

[2]Code 613.3, NASA Goddard Space Flight Center, Greenbelt, MD, USA

[3]Code 610.1, NASA Goddard Space Flight Center, Greenbelt, MD, USA

[4]Code 613.1, NASA Goddard Space Flight Center, Greenbelt, MD, USA

Corresponding Author – E. Nowottnick – epnowott@atmos.umd.edu

Abstract

Saharan dust was observed over the Caribbean basin during the summer 2007 NASA Tropical Composition, Cloud, and Climate Coupling (TC^4) field experiment. Airborne Cloud Physics Lidar (CPL) and satellite observations from MODIS suggest a barrier to dust transport across Central America into the eastern Pacific. We use the NASA GEOS-5 atmospheric transport model with online aerosol tracers to perform simulations of the TC^4 time period in order to understand the nature of this barrier. Our simulations are driven by the Modern Era Retrospective-Analysis for Research and Applications (MERRA) meteorological analyses. We evaluate our baseline simulated dust distributions using MODIS and CALIOP satellite and ground-based AERONET sun photometer observations. GEOS-5 reproduces the observed location, magnitude, and timing of major dust events, but our baseline simulation does not develop as strong a barrier to dust transport across Central America as observations suggest. Analysis of the dust transport dynamics and lost processes suggest that while both mechanisms play a role in defining the dust transport barrier, loss processes by wet removal of dust are about twice as important as transport. Sensitivity analyses with our model showed that the dust barrier would not exist without convective scavenging over the Caribbean. The best agreement between our model and the observations was obtained when dust wet removal was parameterized to be more aggressive, treating the dust as we do hydrophilic aerosols.

1. Introduction

During boreal summer, Saharan dust is transported to the Caribbean and northern South America by the prevailing tropical easterly winds [Karyampudi et al., 1999; Carlson and Prospero, 1972]. Mineral dust aerosols influence Earth's radiation budget directly through the scattering and absorption of light [Zhu et al., 2007; Haywood et al., 2003; Sokolik and Toon, 1996] and indirectly by serving as cloud condensation nuclei (CCN) [Rosenfeld et al., 2001] and ice nuclei [DeMott et al, 2003] and so affecting the properties of clouds. Dust aerosols are thought to modulate tropical cyclogenesis over the tropical North Atlantic by modifying wind fields during development and reducing sea surface temperatures through the absorption of short wave radiation [Lau and Kim, 2007; Dunion and Velden, 2004]. Additionally, insoluble iron in dust aerosols can be converted into a soluble form via photochemistry and cloud processing [Hand et al., 2004; Kieber et al., 2003; Desbouefs et al., 2001; Zhu et al., 1997], which when deposited at the Earth's surface can serve as a nutrient source for aquatic and terrestrial ecosystems [Mahowald et al., 2005; Jickells et al., 2005; Falkowski et al., 2003].

An apparent barrier to dust transport from the Caribbean into the eastern Pacific was suggested by aircraft observations made during July-August, 2007, NASA Tropical Composition Cloud and Climate Coupling (TC^4) field campaign [Toon et al., 2010]. We have identified this Central American dust barrier as a persistent feature in satellite imagery during the boreal summer. While other studies have focused on the broader transport and deposition of dust in the Caribbean [Kaufman et al., 2005; Mahowald et al., 1999, Tegen and Fung, 1995; Duce et al., 1991], we are not aware of any studies identifying this barrier or its causes. We find this barrier is also present in chemical transport model simulations of Saharan dust transport, but that the ability of the model to reproduce the observations is sensitive to the treatment of dust loss processes.

In this paper we explore the controls on establishing and maintaining the observed Central American dust transport barrier, in particular exploring the relative roles of atmospheric dynamics and dust removal processes. We describe our aerosol transport model in Section 2. We present the Central American dust barrier and evaluate our simulated dust distributions using satellite observations from the Moderate Resolution Imaging Spectroradiometer (MODIS) and the Cloud-Aerosol Lidar with Orthogonal Polarization (CALIOP), airborne observations from the Cloud Physics Lidar (CPL), and ground-based observations from the Aerosol Robotic Network (AERONET) (Section 3). We then explore the cause of the Central American dust barrier by analyzing the dynamical and loss transport pathways of the dust in this region (Section 4). We additionally explore the sensitivity of our analyses to uncertainties in our parameterization of dust loss through wet processes (Section 5). We discuss our conclusions in Section 6.

2. Model Description

Our aerosol transport model is based on the Goddard Earth Observing System (GEOS-5) model, the latest version of the NASA Global Modeling and Assimilation Office

(GMAO) earth system model. GEOS-5 contains components for atmospheric circulation and composition (including atmospheric data assimilation), ocean circulation and biogeochemistry, and land surface processes. Components and individual parameterizations within components are coupled under the Earth System Modeling Framework (ESMF) [Hill et al. 2004]. The GEOS-5 earth system model serves as a state-of-the-art modeling tool for studying climate variability and change, and provides research quality reanalyses for use by NASA instrument teams and the scientific community. In addition to traditional meteorological parameters (winds, temperatures, etc.) [Rienecker et al. 2008], GEOS-5 includes modules representing the atmospheric composition, notably aerosols [Colarco et al. 2010] and tropospheric/stratospheric chemical constituents [Pawson et al. 2008], and includes the impact of these constituents on radiative processes within the atmosphere.

GEOS-5 has the capability to run at various horizontal spatial resolutions, from 4° x 5° latitude by longitude for long climate integrations to ~3 x 3 km^2 using advanced dynamical cores. The version we use here is run at 0.5° x 0.625° latitude by longitude, to match the spatial resolution of the meteorological analyses used to drive our simulations. The model has 72 vertical layers distributed in a hybrid coordinate system that is terrain following near the surface and transforms to pressure coordinates near 180 hPa, with a model top at about 85 km.

GEOS-5 can be run as a climate model or in a data assimilation stream. Here, we exploit the GEOS-5 capability to "replay" from a prior data assimilation run. This functions as a data assimilation run in that the model makes a forecast to the analysis time (typically every six hours), however, rather than performing the data assimilation step at that point, the model dynamical state (winds, pressure, temperature, and specific humidity) is simply replaced by fields from the assimilation data set. In our case we use fields from the Modern Era Retrospective Analysis for Research and Applications (MERRA) [Rienecker et al., 2011] analysis, available every six hours at a spatial resolution of 0.5° x 0.625° latitude by longitude.

The aerosol module in GEOS-5 is based on the Goddard Chemistry, Aerosol, Radiation, and Transport (GOCART) model [Chin et al. 2002], as previously integrated into an earlier version of the GEOS model framework [Colarco et al., 2010]. GOCART provides a treatment of five tropospheric aerosol species (dust, sea salt, black carbon, organic carbon, and sulfate), including their sources, sinks, and chemistry. Our treatment of dust follows from GOCART and the description given in Nowottnick et al. [2010]. The dust size distribution is partitioned into five non-interacting size bins spaced between 0.1 and 10 um radius. Dust mobilization follows from Ginoux et al. [2001] with sources preferentially located in large-scale topographic depressions (see also Prospero et al [2002]). Dust losses are through dry and wet removal processes, including turbulent dry deposition, sedimentation, and wet removal by large-scale and convective cloud systems. Further details of our treatment of dust, including dust optics, are provided in Nowottnick et al. [2010] and Colarco et al. [2010].

3. Evidence for the Central American dust barrier and model evaluation

To evaluate Saharan dust transport to the Caribbean and understand the Central American dust barrier we performed a baseline GEOS-5 replay simulation using the MERRA analyses. We simulate all aerosol types with radiative feedback to represent the effect of aerosol absorption and scattering (direct effect) on the atmosphere. After 75 days of model spin-up, we conduct our simulation from June 15, 2010 through August 31, 2010.

3.1 Data Sources

In this section we introduce the observational data sources that show evidence of the Central American dust barrier and which we use to evaluate dust transport in GEOS-5 during TC^4.

3.1.1 MODIS

The Moderate Resolution Imaging Spectroradiometer (MODIS) was launched on December 12, 1999 aboard the Terra spacecraft. A second MODIS instrument was launched on the Aqua satellite as a part of the NASA A-Train on May 4, 2002. The MODIS instruments provide multispectral observations of the Earth system using 36 channels at 10:30 AM (Terra) and 1:30 PM (Aqua) local time. MODIS aerosol retrievals are made at a spatial resolution of at 10 x 10 km^2 using separate retrieval algorithms for ocean and land. Over oceans, the MODIS algorithm uses retrieved radiances from six channels (550, 660, 870, 1240, 1630, and 2130 nm) to provide aerosol information at seven wavelengths, using the six retrieved channels and an additional fitted wavelength at 470 nm [Remer et al., 2005]. Over land, an empirical relationship between radiance retrievals at two visible channels (470 and 660 nm) and one near-IR channel (2130 nm) is used to determine the surface reflectivity to provide aerosols properties at 470, 550, and 660 nm [Remer et al., 2005]. For our analysis, we use MODIS aerosol optical thickness (AOT) observations at 550 nm from collection 5.1. MODIS provides semi-quantitative quality assurance (QA) flags, where QA ranges in integer from QA=0 (low confidence in aerosol retrieval) to QA=3 (high confidence in retrieval). Over land we aggregate only highest quality (QA=3) retrievals, whereas over ocean we aggregate all retrievals but weight them by their respective QA flag value, similar to the MODIS canonical Level 3 gridded product [Levy et al., 2009].

3.1.2 AERONET

The Aerosol Robotic Network (AERONET) of ground-based sunphotometers provide measurements of direct solar beam extinction every 15 minutes at 340, 380, 440, 500, 670, 870, and 1020 nm to provide AOT measurements at 440, 670, 870, and 1020 nm with an accuracy of +/-0.015 [Holben et al., 2001]. AERONET utilizes principle plane and almuncantar scans to invert aerosol properties and to determine size information [Dubovik and King, 2000]. To determine the AERONET AOT at 550 nm for comparison to our model, we first determine the 470-870 nm Angstrom parameter α, defined:

$$\tau_1 = \tau_2 \left(\frac{\lambda_1}{\lambda_2} \right)^{-\alpha} \quad (1)$$

where τ_1 and τ_2 are AERONET AOT values at $\lambda_1 = 470$ nm and $\lambda_2 = 870$ nm, respectively. Once the Angstrom parameter is determined, we use Equation 1 to determine τ at $\lambda = 550$ nm. For evaluation of our model, we use AERONET version 2, Level 2 cloud-screened and quality-assured daily averaged AOT values [Smirnov et al., 2000] at AERONET sites that are near and downwind of the source region (Figure 1).

3.1.3 CALIOP

The Cloud-Aerosol Lidar with Orthogonal Polarization (CALIOP) was launched onboard CALIPSO on April 28, 2006 as part of the NASA A-Train. CALIOP is a two-channel (532 and 1064 nm) spaceborne lidar that provides profiles of cloud and aerosol properties along the satellite subpoint [Vaughan, 2005]. CALIOP has a temporal resolution of 20.16 Hz and vertical resolution that varies from 30 m in the troposphere up to 60 m at higher altitudes. Because CALIOP is an active instrument, it provides both a daytime (1:30 pm local time) and nighttime (1:30 am local time) measurement. CALIOP sends out polarized light at 532 nm and is equipped with sensors that measure the parallel and perpendicular components of the backscattered signal. The standard CALIOP retrieval provides measurements of total attenuated backscatter at each channel [Vaughan, 2005]. However, polarization information and spectral variation of the backscatter can be used to infer the presence of aerosols and their type [Vaughan, 2005] In the CALIOP algorithm, backscatter from aerosols is differentiated from clouds by defining a lidar color ratio ($\beta_{1064nm} / \beta_{532nm}$). At visible wavelengths, aerosols exhibit spectral variation while clouds do not, therefore a lidar color ratio that is approximately one is used to identify clouds [Vaughan, 2005]. Once aerosols are differentiated from clouds, polarization properties can be used to infer aerosol type. Non-spherical aerosols such as dust are depolarizing and contribute to signal return in both the perpendicular and parallel planes. Spherical aerosols are not strongly polarizing and scatter predominantly in the parallel plane. Therefore, a depolarization ratio ($\beta_{perpendicular} / \beta_{parallel}$) can be defined to identify the presence of non-spherical aerosols. For our analysis, we use CALIOP version 3.01 data, which offers an improved technique for the daytime 532 nm total attenuated backscatter calibration relative to previous versions.

3.1.4 CPL

The Cloud Physics Lidar (CPL) is a multi-pulse lidar that has provided observations during several NASA field campaigns [McGill et al., 2004; McGill et al., 2000]. During TC^4, CPL flew on the NASA ER-2 aircraft, providing profiles of total attenuated backscatter on 16 different days. CPL measures backscatter at 3 wavelengths (355, 532, and 1064 nm) with a frequency of 5 kHz and depolarization ratio at 1064 nm [McGill et al., 2002]. Processed CPL data is available with a temporal resolution of 1 s and has a spatial resolution of 30 m in the vertical and 200 m in the horizontal [McGill et al., 2002].

3.2 Evidence of the Central American dust barrier

To illustrate the Central American dust barrier, we show the climatology of July MODIS-Aqua (2003-2010) and MODIS-Terra (2000-2010) land and ocean AOT averaged over latitudes of peak Caribbean dust AOT (10° N - 20° N, see Figure 1) in Figure 2. From this, we see that the Central American dust barrier is a persistent feature, marked by a sharp drop in the AOT west of 80° W. Specifically, during July 2007, the MODIS-Terra AOT drops from 0.375 at 80° W down to 0.2 at 90° W.

Also shown in Figure 2 is the July 2007 AOT from the GEOS-5 model averaged over the same region. For this comparison we sample our modeled aerosol distributions at the times and locations of the MODIS observations, which has been shown to reduce biases between the MODIS and model AOT because of clouds [Colarco et al., 2010]. Over the Caribbean (west of 60° W), the model AOT is comparable to MODIS-Terra. Near the Central American coastline, the model shows evidence of a barrier to dust transport, although not as drastic, decreasing from 0.4 at 80° W to 0.3 at 90° W (Figure 2). This suggests that either our removal processes or atmospheric dynamics that drive transport might not be correct over this region of the Caribbean and will be further explored in Section 5. Despite this, the model shows evidence for a barrier to dust transport that corresponds with the Central American coastline.

3.3 Model Evaluation

Here we evaluate the location, timing, and magnitude of dust events simulated in our model with AOT observations from MODIS-Aqua and AERONET and vertical profile observations from CPL and CALIOP.

Figure 3 shows July 2007 monthly means of total AOT from MODIS-Aqua and our simulation (sampled at MODIS-Aqua observations points as described above). Off the west coast of North Africa, the model has the peak AOT in the same location as the sensor, but at a greater magnitude. Moving west across the tropical North Atlantic, the model matches the observed dust plume location and width, and the magnitude of AOT becomes more comparable with observations. Owing to improvements in the model physics and the MERRA analyses, GEOS-5 does better transporting dust from the Saharan source region to the Caribbean relative to previous versions of the model [Colarco et al., 2010; Nowottnick et al., 2010]. However, the model extends its dust plume somewhat into the eastern Pacific (90° – 95° W), while MODIS-Aqua AOT values are constrained to the Caribbean. This feature is also seen in Figure 2, where the model representation of the Central American dust barrier is not as pronounced as observed by MODIS-Terra.

To evaluate the timing of simulated dust events in the model we compare our For each AERONET site, we compare the observations to simulated total AOT values from the model grid box that contains the location of the site and calculate mean AOT and square of the Pearson correlation (r square) values on days when AERONET data is available (Figure 4). During TC^4, we have data from three AERONET sites near the source region (Ras El Ain, La Laguna, and Capo Verde) and one site downwind (Cape San Juan).

At the Ras El Ain site, the model has excellent agreement with the magnitude and the timing of observed dust events, marked by comparable mean AOT values and a high correlation coefficient ($R^2 = 0.71$). On the island of Tenerife, the model is well correlated with the elevated La Laguna site ($R^2 = 0.62$), but is somewhat larger in magnitude. AERONET AOT values exhibit more variability than at Ras El Ain, as passing dust events cause a peak in AOT for 2-3 days and then return to almost zero. The model reproduces the daily variability when compared to AERONET, but simulate a greater AOT when dust events are observed. At the Capo Verde site, located downwind of a major Saharan dust source, the model simulates a slightly higher mean AOT value and is moderately correlated ($R^2 = 0.46$) with AERONET. The lower correlation might be the result of fewer coincident data points between AERONET and model, likely requiring more observations for a more meaningful evaluation of the model at this location. Downwind of the Saharan source region at the Cape San Juan site, the model is well correlated ($R^2 = 0.56$) with AERONET, matches the timing of transported dust events, and has a mean AOT value that is nearly identical to the mean AERONET value.

Overall, GEOS-5 accurately simulates the timing and magnitude of dust events near the Saharan source region and in the Caribbean during the TC^4 field campaign as compared to the AERONET observations. This contrasts with our comparison to MODIS-Aqua, where the model generally simulated a higher AOT, particularly just downwind of the Saharan source region. The MODIS and AERONET datasets are complementary and have their respective advantages. While MODIS provides a great deal of spatial coverage, there are uncertainties in the retrieved AOT due to uncertain aerosol optical properties, surface characterization, and cloud contamination. On the other hand, AERONET provides a direct measurement of AOT and has a much higher temporal coverage (multiple observations per day). When comparisons to AERONET are combined with those to MODIS-Aqua, we find that the model captures the shape, magnitude, and timing of dust plumes during the TC^4 timeframe.

During TC^4, a Saharan dust plume was observed over the Caribbean on 19 July with the CPL flying on the NASA ER-2 aircraft. Using CALIOP, we tracked this dust event from the Saharan source region (14 July) to the Caribbean (19 July) to evaluate our simulated vertical dust distributions during transport (Figure 5). For an accurate comparison, we sampled GEOS-5 along the CALIPSO track at the model synoptic time nearest to the daytime CALIOP measurement. Shown in Figure 6 are GEOS-5 comparisons to CALIOP 532 nm total attenuated backscatter and feature mask from 14 July to 19 July. On 14 July, CALIOP observes a thick, elevated dust plume located from 2-5.5 km that extends from 10° - 26° N. The model captures the latitude extent of the dust plume observed by CALIOP, but is lower in altitude ranging from 1-5.5 km. A limitation of CALIOP is that its signal becomes attenuated towards the surface when it encounters thick aerosol plumes. On this day, the CALIOP signal might be partially attenuated at low altitudes, so the CALIOP data may suggest the lowest edge of the dust plume is at a higher altitude than it actually was. In the CALIOP layer identification product, low-level marine clouds are observed north of 15° N below 1 km. While we only show extinction from aerosols, the influence of these clouds can be seen in the aerosol total extinction where the aerosols in this region have swelled in the marine boundary layer and are marked by high extinction values. Moving farther from the Saharan source region, the edge of a dust event is observed on 15 July. CALIOP observes an elevated, thick layer of dust that extends from 2-5 km between 11° - 24° N, which is well represented in the model. Further downwind on 17 July, the model matches the observed horizontal extent and altitude of the observed dust plume. The simulated dust plume extends down to the surface into a region where CALIOP identifies a thin layer of maritime clouds, making it difficult to determine whether the lower extent of the simulated plume is correct. On 19 July, the model captures the narrow north-south width and low-altitude dust plume observed below 3 km by CALIOP, although clearly the observations are impacted by the presence of mid- and low-level clouds. In general, we see for this case that GEOS-5 is capturing similar dust plume features to the CALIOP observations during this time period.

Figure 7 shows the spatial distribution of AOT at 550 nm retrieved from MODIS-Aqua and GEOS-5 at 18Z, with the ER-2 flight track overlaid on 7/19. The flight originated from Costa Rica, heading southwest over the Pacific Ocean to 90° W, then turned around and headed northeast back towards Costa Rica. The aircraft continued past Central America over the Caribbean Sea to 75° W and then headed southwest back to Costa Rica. During the flight, CPL provided an approximately east-west transect of total attenuated backscatter that extends from the Pacific Ocean into the Caribbean. Comparing the model to MODIS-Aqua on this day, the model matches the observed AOT location and magnitude over the Caribbean. Over the Pacific Ocean MODIS-Aqua is partially obscured by clouds, but the model shows a majority of the model AOT confined to the

Caribbean and over Central America. This phenomenon is more clearly seen in the CPL profile of the 532 nm total attenuated backscatter and column AOT when compared to GEOS-5 profiles of extinction and AOT at 550 nm that have been sampled along the ER-2 track at the nearest model synoptic time on 7/19 (Figure 7). Although the CPL signal is frequently attenuated by clouds over the Pacific and only occasionally over the Caribbean, both CPL and GEOS-5 provide an illustration of the Central American dust barrier along the eastern coastline of Costa Rica (9° N, 84° W, marked by a mountain). To avoid cloud contributions to the AOT, we compare the column AOT from 5 km to the surface for CPL and GEOS-5 (Figure 7). CPL observes high AOT values over the Caribbean, and a sharp decrease in AOT that corresponds with the Central American coastline. A similar feature is seen in the simulated AOT but at a lower magnitude and as in Figure 2, the representation of the Central American dust barrier is not as well defined, indicating that our transported dust loading might be too low on this day.

4. Controls on Saharan Dust During Transport

To understand the cause of the Central American dust barrier, we must understand the roles of the controls on dust distributions during transport. Once emitted from the source region, dust is further lifted into the atmosphere through dry convection and turbulent eddies to form an elevated layer, often penetrating into the so-called Saharan Air Layer (SAL) of hot, dry air [Karyampudi, 1999]. During summer months, a surface north-south temperature gradient forms between the hot Sahara and the relatively cooler Sahel [Cook et al., 1999]. Through thermal wind balance, this leads to the summertime African

Easterly Jet (AEJ). During AEJ formation, the SAL converges on the north side of the AEJ axis and is then transported along the north side of the AEJ, delivering dust to the Caribbean. During the journey from the Sahara to the Caribbean, dust distributions are controlled by both dynamical and loss processes. Atmospheric dynamics controls the direction and magnitude of the transported dust mass flux or flow, while loss processes control the overall dust burden. Therefore, we suspect that the Central American dust barrier is caused by increases in wet removal, a change in transport direction resulting from a shift in the prevailing atmospheric dynamics, or some combination of both.

Ideally, we would have airborne measurements while tracking several dust plumes to help understand cause of the Central American dust barrier. Unfortunately, measurements of this sort are extremely limited. However, from our comparisons to observations of mean dust plume position, event timing, and vertical distributions near and downwind of the Saharan source region, GEOS-5 provides a reasonable representation of dust distributions during the TC^4 timeframe, while simulating the aforementioned processes that are not easily measured. The accuracy of our simulated wet removal processes are directly linked to our ability to accurately simulate the timing and intensity of precipitation events. Figure 8 shows the July 2007 mean precipitation (mm day^{-1}) from the Global Precipitation Climatology Project (GPCP) [Huffman et al., 2009; Adler et al., 2003] and GEOS-5. GPCP provides monthly mean precipitation data at 1° x 1° resolution using rain gauges, microwave satellite observations from the Special Sensor Microwave Imager (SSM/I), and infrared satellites observations from many global geostationary satellites [Adler et al., 2003]. The precipitation patterns in GEOS-5 are generally consistent with GPCP, matching peak values located over Central and South America. However, GEOS-5 produces a broad area of convective precipitation over the Caribbean that is not seen in the GPCP data. Over the Caribbean, the average GEOS-5 precipitation rate is 5 mm day^{-1} while the average GPCP precipitation rate is 1.5 mm day^{-1}. This presents an interesting feature of the model. Figure 2 suggests that our removal rates are not aggressive enough in removing dust, particularly in the region of the Central American dust barrier. However, on average, our precipitation rate is greater by a factor of three (Figure 8). This quandary suggests that the relationship between precipitation and wet removal is not strong enough in our model. We could, alternatively, simply rescale our dust emissions lower, which would remove most of the bias seen in Figure 2, but crucially this would not produce the abrupt dust barrier evident in the data at approximately 90° W.

In addition to possible errors in our representation of loss processes, our simulated dust distributions are sensitive to atmospheric dynamics. By using a replay simulation, we are providing the model with assimilated winds, so that it will be forced with actual dynamics at each synoptic time. Our estimation of dust transport is therefore sensitive to our ability to reproduce the actual dynamical state and will be limited by errors in the representations of advection, planetary boundary layer mixing, and convective mixing. In addition to sensitivities to the internal dynamical processes, simulated dust distributions will also be sensitive to the accuracy of observations used in the analysis. Despite these potential sources of error, our July 2007 simulated dust distributions are comparable to MODIS-Aqua, AERONET, and CALIOP, as shown in Section 3.

Therefore, we use our dust distributions from GEOS-5 to understand the relative roles of the processes that control the Central American dust barrier.

4.1 Dust Mass Budget

We begin our investigation of the controls on the Central American dust barrier by employing the vertically integrated mass divergence form of the continuity equation for mean values from July 2007:

$$\frac{\partial q}{\partial t} = (P - L) + \nabla \cdot \vec{Q} \qquad (2)$$

where q is the column dust loading defined:

$$q = \sum_{z=0}^{z=top} \gamma * \rho_{air} * dz \qquad (3)$$

and $\vec{Q}$ is the vertically integrated dust mass flux:

$$\vec{Q} = \begin{array}{l} \sum_{z=0}^{z=top} \gamma \cdot \rho_{air} \cdot u \cdot dz \cdot \hat{i} \\ + \sum_{z=0}^{z=top} \gamma \cdot \rho_{air} \cdot v \cdot dz \cdot \hat{j} \end{array} \qquad (4)$$

Here, γ is the dust mass mixing ratio (kg kg^{-1}), ρ_{air} is the atmospheric air density (kg m^{-3}), u and v are the east-west and north-south components of the wind field (m s^{-1}), and dz is the thickness (m) of each model layer in the vertical column.

After integrating in the vertical, Equation 2 has three terms: the storage term ($\frac{\partial q}{\partial t}$), the production-loss (P – L) term, and the divergence, or transport, term ($\nabla \cdot \vec{Q}$). The storage term represents the net local change in the dust column loading, the P – L term is defined as the sum of the column emission fluxes minus fluxes due to dry and wet removal, and the transport term represents any dust column convergence and divergence resulting from transport. All terms in Equation 2 are in flux form and have the units (kg m^{-2} s^{-1}). Equation 2 can be interpreted as any accumulation of dust mass within an atmospheric column results from the sum of the net production minus loss and dust import/export via transport. Figure 9 shows the July 2007 monthly mean storage, P – L, and transport terms. We analyze each term separately to understand their respective influence on our simulated dust distributions over the Caribbean. Our analysis of Equation 2 uses monthly mean components that have been computed from instantaneous model output at every 3 hours; thus, the fields examined include both the mean flow and the contribution from transient eddies.

4.1.1 Storage Term

At each grid cell, the storage term represents the mean local change in the column dust loading q (kg m^{-2}) (Equation 3). During July 2007, the largest variations in the dust column loading occur away from regions of semi-persistent dust flow (Figure 9). This can be seen north of 20° N off the west coast of North Africa during July 2007, where removal rates are small (Figure 9). Eventually, this dust will be removed from the atmosphere via loss processes or transport. Over the Caribbean, the storage term is significantly less than the P – L and transport terms, indicating that the other terms are in near-balance over this region. Over longer time periods, we expect the storage term to approach zero, as deviations in the mean dust flow will become less significant and averaged out. In this case, the P – L term will balance the transport term.

4.1.2 P – L Term

The mean P – L term for July 2007 shows positive values over the global source region and negative values downwind, corresponding to regions where emissions and losses prevail, respectively (Figure 9). Once dust is emitted from the source region, the total atmospheric burden is controlled by losses through dry and wet removal processes. In the Atlantic, losses peak immediately downstream of the source region, although a broad area of high dust losses carries into the Caribbean.

Figure 10 shows the relative contributions of our modeled dust loss processes as a function of distance from the source region. By mass, gravitational sedimentation is the dominant removal process near the Saharan source region, as the largest, most massive dust particles fall quickly from the atmosphere. Sedimentation becomes less efficient further downwind as the largest particles are removed. Wet removal becomes the dominant loss process, first via large-scale precipitation immediately west of the source region and then through convective precipitation in the western Caribbean and near Central America. This region where convective removal dominates coincides with the location of the Central American dust barrier.

4.1.3 Transport Term

The transport term represents any column accumulation or loss of dust from the divergent component of the transported dust mass flux. To analyze the contribution of transport to Equation 2, we begin with our vertically integrated dust mass flux $\vec{Q}$ (kg m^{-1} s^{-1}) (Equation 4). Because dust is typically located at low altitudes, $\vec{Q}$ will be weighted toward the mass concentration and the near-surface wind direction and magnitude.

Consider the Helmholtz decomposition [Brown, 1991]:

$$\vec{Q} = \vec{Q}_{rot} + \vec{Q}_{div} \qquad (5)$$

where $\vec{Q}_{rot}$ and $\vec{Q}_{div}$ are the rotational and divergent components of the vertically integrated mass flux vector $\vec{Q}$, with $\nabla \cdot \vec{Q}_{rot} = 0$ and $\nabla \times \vec{Q}_{div} = 0$ by definition. The corresponding mass flux streamfunction ψ and velocity potential χ can be obtained by solving Poisson's equations [Brown, 1991]:

$$\nabla^2 \Psi = \nabla \cdot \vec{Q}_{div} \qquad (6)$$

$$\nabla^2 \chi = \hat{k} \cdot \nabla \times \vec{Q}_{rot} \qquad (7)$$

from which we obtain the divergent and rotational components of $\vec{Q}$:

$$\vec{Q}_{rot} = -\frac{\partial \Psi}{\partial y}\hat{i} + \frac{\partial \Psi}{\partial x}\hat{j} \qquad (8)$$

$$\vec{Q}_{div} = \frac{\partial \chi}{\partial x}\hat{i} + \frac{\partial \chi}{\partial y}\hat{j} \qquad (9)$$

The rotational component depicts the recirculation of dust in the atmosphere, while the divergent component of the vertically integrated mass flux is associated with the P – L process ($\nabla \cdot \vec{Q}_{div} = \nabla \cdot \vec{Q}$) (Equation 2). Shown in Figure 11 are the July 2007 mean streamfunction and velocity potential contours with the rotational and divergent dust flow vectors overlaid. We recall that the rotational component of the dust flow is proportional to the curl of the streamfunction; therefore, rotational flow will be strongest where streamlines are closest. By definition, the rotational flow will be cyclonic surrounding relative minima of the streamfunction, and anti-cyclonic surrounding the relative maxima. We see strong rotational dust flow leaving the Sahara as part of the SAL and riding on the northern side (15° – 25° N) of the AEJ across the Atlantic Ocean. In this region, the rotational component of the dust flow is strong for two reasons: 1) dust concentrations are high within the SAL and 2) strong, non-divergent easterlies within the AEJ persist. The effect is a narrow band (15° – 25° N) of strong rotational flow that transports dust from the Sahara to the Caribbean. Upon reaching the Caribbean, the rotational flow weakens because: 1) dust loss processes have reduced the overall dust load during transport and 2) easterly wind speeds are reduced. Additionally, the flow direction shifts from primarily westward to north-westward over the Caribbean as it is now influenced by the Azores subtropical high-pressure system that exists over the Atlantic Ocean. The rotational dust flow eventually turns eastward and returns dust back to the Saharan source region. Thus, when following a constant streamline, the rotational component of Saharan dust flow is an anti-cyclonic recirculation, where dust leaves the source region as part of the AEJ and returns with the westerlies as part of the Azores

High. A similar—but weaker—cyclonic feature is seen south of 15° N, transporting dust to South America.

The divergent component of the flow is proportional to the gradient of the velocity potential. Therefore, regions of divergence correspond to relative minima of the velocity potential correspond, while regions of convergence correspond to relative maxima. In Figure 11, we see a dipole in the divergent flow field between the Saharan source region and the Caribbean. Over the source region strong divergent flow persists, as a divergent component to the dust flow is required for dust to leave the source region. During transport, the divergent flow is significantly reduced and there is a broad, region of convergence over the Caribbean where loss processes prevail. The significant reduction in the divergent flow can be the result of a weakening of the wind field or a reduction in the dust burden caused by the various loss processes during transport. As previously mentioned, the divergence of the divergent flow ($\nabla \cdot \vec{Q}_{div}$) is the transport term in Equation 2. In Figure 9, as expected, the July 2007 transport term is positive (divergent) over the source regions, as dust is transported outward from the sources. Downwind of the Saharan source region, the transport term is negative (convergent), which corresponds with the convergent flow field in Figure 11. One striking feature of the divergence field is that it aligns with the P – L term in regions where production and loss occur. Because these regions have a semi-persistent flow of dust for this month and the storage term is small, there is a near-balance between the transport and P – L terms. Thus, over these regions, regions of dust emission (P – L > 0) correspond with divergent outflow (positive transport term) and regions of dust loss (P – L < 0) correspond with convergent inflow (negative transport term). We expect that convergent flow increases dust loss rates in two ways. First, the convergent flow will accumulate dust within the atmospheric column. This accumulation will increase the potential for removal in regions where the storage term is small. Second, we find vertical motion over convergent regions (not shown), which is associated with convection. This second process is more relevant for wet removal as we expect greater wet deposition and scavenging rates in the presence of precipitation and clouds.

Despite the link between P – L and divergent flow, it is clear that rotational flow has a greater magnitude and is in a different direction (predominantly westward) than the divergent flow (predominantly eastward). However, this alone does not lend much insight into any influences that transport might have on the Central American dust barrier. In addition to the effects of loss processes, the dust barrier could be influenced by a slight change to the flow field over the Caribbean or a combination of the rotational and divergent components. To better understand this, we further break the rotational and divergent components into their east-west and north-south components. Figure 12 shows the east-west and north-south total, rotational, and divergent flow components. Over the Caribbean, the rotational component of the east-west flow is strongly westward while the divergent component is weakly eastward. Despite cancellation between the two components near the coast of Costa Rica, the net east-west flow is westward and acts to transport dust across Central America. The north-south flow for the rotational component shifts from southward to northward near 12.5° N over the Caribbean, while the divergent flow shifts from northward to southward flow at 17.5° N. However, the net north-south flow is northward over the entire Caribbean. Thus, there is a northward turning of the dust flow as it enters the Caribbean, which when combined with the net westward flow causes a northwestern migration of the overall dust flow and serves as a possible explanation of the Central American dust barrier.

4.2 Loss Processes vs. Transport

We investigate the dust mass budget in the latitude band of peak dust AOT (10° – 20° N) to understand the relative roles of dust loss processes and transport in the Central American dust barrier. Figure 13 shows the mass of dust removed from loss processes, from transport out of the northern (20° N) and southern (10° N) sides of the latitude band, and the change in the east-west mass flux (flux in minus flux out) as a function of longitude. To obtain the amount of dust lost via removal, we integrate the P – L rates spatially and temporally and sum over the latitude band at each longitude (black curves in Figure 13). To quantify the net north-south dust mass flux out of the band, we subtract the net spatially and temporally integrated north-south dust flux at 20° N from that at 10° N at each longitude (Figure 13). To obtain the change in the east-west mass flux, we first integrate the net east-west component of the dust flow spatially and temporally at each grid box. The change in the east-west mass flux is then determined by differencing the east-west flow in the westward direction and then summing along all latitudes (Figure 13). Negative mass values in Figure 13 correspond with net loss via removal processes or transport out of the latitude band, or a reduction in the westward mass flux. It should be noted that the sum of the net north-south mass flux and the change in the westward mass flux is the divergence term in Equation 2. This sum is approximately equal to the mass of dust removed by loss processes, with any residual related to the storage term.

Over the Caribbean, removal from loss processes and northward transport were shown to serve as possible causes of the Central American dust barrier. In Figure 13, the longitudes of the Central American dust barrier (80° - 90° W) correspond with increases in dust mass loss and northward transport. To quantify their relative contributions, we integrate the production-loss and north-south transport curves in Figure 13 over the region of the Central American dust barrier. From this, we estimate that loss processes remove 1.67 Tg of dust while the north-south dust flow transports 1.46 Tg of dust out of the Central American dust barrier region during July 2007 (Table 1).

Based on these estimations, it is clear that both loss processes and atmospheric dynamics have a contribution to the Central American dust barrier. Of the two processes, dust loss from removal processes has a slightly greater contribution (53%) to the Central American dust barrier than northward transport (47%).

5. Discussion

We have shown that loss processes have a greater contribution towards the Central American dust barrier than northward transport for July 2007. From Figure 10, it is clear that wet removal by large scale and convective scavenging dominate the loss processes downwind of the Saharan source region between 10° – 20° N and serve as the major pathways for dust removal over the Caribbean. However, as discussed in Section 3.2.1, we suspect that our wet removal rates are not aggressive enough over the Caribbean and serves as the cause of our weaker representation of the Central American dust barrier in Figure 2. To explore the controls of wet removal on our transported dust distributions, we perform additional simulations of July 2007 where we modify our parameterization of wet removal processes relative to our baseline simulation setup.

Table 1 presents a budget analysis for our baseline simulation, as well as the sensitivity analyses we will discuss here. Included are the dust mass removal by loss processes, north-south transport, and their contribution to the Central American dust barrier. Also shown are the 10° – 20° N net east-west mass transported across the planes at 80° W and 90° W and their difference. This difference, when combined with the north-south transport is the mass divergence and should approximately balance the mass removed by loss processes, with any residual attributable to the storage term in Equation 2. Table 1 lists a dust mass barrier efficiency of the Central American dust barrier defined as the difference between the 10° – 20° N net east-west transported dust mass at 80° W (flow in) from that at 90° W (flow out) divided by the transported dust mass at 80° W (flow in). Additionally, after sampling consistently with MODIS-Terra, Table 1 lists a total AOT barrier efficiency and a coarse mode (dust plus sea salt) AOT efficiency that can be compared to the MODIS coarse mode AOT after averaging from 10° – 20° N.

Our baseline simulation has a dust mass barrier efficiency of 0.36, meaning that the Central American dust barrier removes 36% of the dust mass between 80° W to 90° W

(Table 1). Our baseline simulation has a total AOT barrier efficiency of 0.21 and a coarse AOT efficiency of 0.17. Comparisons to MODIS-Terra show that our removal rates are not aggressive enough, as MODIS-Terra has a total AOT barrier efficiency of 0.37 and coarse AOT barrier efficiency of 0.30 (Table 1).

As our model does not include a detailed representation of aerosol-cloud-precipitation interactions, we parameterize aerosol wet removal in terms of the model grid box convective updraft mass flux (for convective scavenging) and precipitation rate (for large scale wet removal). An efficiency factor is assigned to each aerosol species that represents its susceptibility to wet removal (i.e., its hygroscopicity) [Colarco et al. 2010]. For dust we have assumed its wet removal efficiency is approximately half as efficiency as for hydrophilic carbonaceous and sulfate aerosols. In our first sensitivity test we double the dust convective scavenging efficiency so that it is equivalent to that for hydrophilic aerosols. In Figure 13, we see that doubling the convective scavenging rate increases the mass of dust lost to removal while reducing the north-south and east-west dust flow. If we integrate along our longitudes of the Central American dust barrier, doubling the convective scavenging rate increases the loss contribution to 61% (1.90 Tg) and reduces the contribution by northward transport to 39% (1.24 Tg), increasing the mass barrier efficiency to 0.48 (Table 1). Figure 14 shows the MODIS-Terra sampled AOT from our baseline and sensitivity tests, the ratio of the MODIS-Terra and simulated AOT, and the slope of the AOT ($\Delta\tau/\Delta x$). After doubling the convective scavenging rate, we see a reduction in the high AOT bias in the model and improvement in the slope of AOT as a function of longitude (Figure 14). This corresponds with a significant improvement in the representation of the Central American dust barrier as the simulated AOT reduces from 0.34 at 80° W to 0.25 at 90° W (Figure 14). This corresponds to greater AOT barrier efficiencies of the total (0.25) and coarse (0.21) representations of the Central American dust barrier.

We performed a second sensitivity test where in addition to doubling the dust convective scavenging rate, we increased the large-scale scavenging rate so that dust wet removal is treated the same as for hydrophilic aerosols. While this further increases the mass of dust lost to removal and reduces the north-south and east-west flow, we find that our simulated dust distributions are more sensitive to modifications to convective scavenging than large-scale scavenging in this region. However, the combined effect of increasing the large-scale and convective scavenging rates consistent with other aerosol types corresponds with an increased contribution from loss processes (66%, 1.97 Tg), a reduced contribution (34%, 1.02 Tg) from northward transport, and an increase in the barrier mass efficiency (0.52) of the Central American dust barrier (Table 1). Treating the wet removal of dust the same as other aerosols yields further improvement in the representation of the AOT magnitude and slope when compared to MODIS-Terra (Figure 14). Over the region of the Central American dust barrier, the simulated AOT reduces from 0.31 at 80° W to 0.23 at 90° W (Figure 14), corresponding with an improved total AOT barrier efficiency of 0.28 and a coarse AOT barrier efficiency of 0.22 (Table 1). Although still not as efficient as indicated by MODIS-Terra, this result suggests that the dust wet removal rates in GEOS-5 are too slow and treating the wet removal of dust in a fashion similar to other (more ostensibly hygroscopic) aerosol types yields better comparisons to observations in regions where wet removal is dominant. Because the representation of the dust barrier improves with increases to the wet removal rates, the contribution from loss processes to the Central American dust barrier is likely greater (66%) than originally estimated from our baseline simulation (53%).

We performed two additional sensitivity tests aimed at understanding if the Central American dust barrier exists when the effects of convective and large-scale scavenging are not simulated. In the first sensitivity test, we did not simulate wet removal from the large-scale scavenging of dust, leaving only convective scavenging as a source of wet removal. As shown in Figure 13, large-scale scavenging over the Caribbean has a small effect on the dust load, as the northward and westward flows are slightly increased and losses are reduced when the effects of large-scale scavenging are not simulated. When we integrate over the longitudes of the Central American dust barrier, we see a shift in the relative significance of northward transport and loss. Northward flow transports 1.85 Tg of dust out of the region (59% of the total removal) while dust losses remove 0.95 Tg of dust (41% of the total removal), corresponding with a barrier mass efficiency of 0.33 (Table 1). When the AOT is sampled consistent with MODIS-Terra, we see a small increase in the magnitude of the AOT and slope from the coast of North Africa (20° W) to Central America (80° W), but there is still evidence of a Central American dust barrier (Figure 14). When the effects of large scale scavenging are not simulated, the total AOT efficiency and coarse AOT efficiency decrease to 0.19 and 0.16, respectively (Table 1). This result is consistent with the simulations already discussed and suggests that large-scale convective scavenging has a small effect to the Central American dust barrier.

In a final sensitivity test, we performed a simulation where the effects of all wet removal (convective scavenging and large-scale scavenging) were not simulated. In Figure 13, we see a large increase in the northward and westward dust flows and a significant reduction in the dust loss. Over the Central American dust barrier region, northward transport accounts for 78% (3.35 Tg) of dust removal from the atmospheric column, while loss processes account for 22% (1.28 Tg), corresponding with a mass barrier efficiency of 0.25 (Table 1). When compared to MODIS-Terra, we see a nearly constant increase in the AOT from the coast of North Africa (20° W) to the beginning of the Caribbean (60° W) (Figure 14). However, over the Caribbean where convective scavenging has the largest contribution to the overall removal (Figure 10), the model AOT relative to MODIS-Terra increases non-linearly (Figure 14) and reduces the total and dust AOT barrier efficiency to 0.17 and 0.13, respectively (Table 1). Finally, when all wet removal processes are not included, there is no evidence of the Central American dust barrier (Figure 14). Therefore, we determine the Central American dust barrier could not exist without convective scavenging. In practice, however, the Central American dust barrier is the result of two processes working in tandem: 1) Loss processes significantly reducing the dust loading during transport and 2) Atmospheric dynamics redirecting the reduced dust flow northward near the Central American coastline.

6. Conclusions

We used the GEOS-5 model to simulate the distribution of aerosols during the period of the NASA TC^4 field campaign (July – August, 2007). In this simulation, we have shown that GEOS-5 simulates dust distributions that are spatially and temporally comparable to MODIS, CALIOP, and AERONET data. Downwind of Africa, GEOS-5 has a similar plume shape to the MODIS observations, but in our baseline simulation overestimates the AOT. GEOS-5 has a better agreement with AERONET AOT values and is well correlated with the AOT time series from sites within and nearby the Saharan source region. GEOS-5 accurately reproduced the latitudinal, longitudinal, and vertical extent of a Saharan dust event during its transport from North Africa to the Caribbean when compared to CALIOP. Over the Caribbean, GEOS-5 AOT magnitude is comparable to MODIS and well correlated with the Caribbean AERONET site, but provided a weak representation of the Central American dust barrier. This feature suggested that our loss processes be explored and possibly adjusted in future implementations of the model.

In a series of sensitivity analyses with our model we explored the relationship between wet removal parameterization and transport in defining the Central American dust transport barrier. The best agreement between our model and the observations was obtained when dust wet removal was treated as we treat the removal of hydrophilic aerosol species. Conversely, we showed that in the absence of dust wet removal there is essentially no dust transport barrier set up in our model. The implication of appealing to an increase in dust wet removal efficiency is that perhaps processing of dust during transport results in a more hydrophilic aerosol. Such an aerosol would likely be more bioavailable to oceanic organisms once it is eventually deposited.

Our analysis shows that both wet removal and transport play a role in creating a semi-permeable barrier to dust transport across Central America into the Pacific. Of the two processes, for our best case simulation we find wet removal has a factor of two greater contribution toward defining the barrier than northward transport. Moreover, of the removal processes, the Central American dust barrier is more sensitive to removal by convective scavenging and is not evident when convective scavenging is not simulated.

Our results should be taken with a few caveats. First, our component analysis is valid for July 2007. While we have shown that the Central American dust barrier is a persistent feature in July (Figure 2), we expect that the barrier will be somewhat sensitive to the variability of inter-annual meteorological conditions over the Central American region. Pfister [2010] found that La Nina conditions in 2007 caused an increase in westward flow and a significant reduction in Caribbean cold clouds and corresponding increase in Pacific cold clouds during the TC^4 field campaign. This suggests that under less anomalous conditions, transported dust would be more confined the Caribbean and the Central American dust barrier would have a greater presence. The presence of the Central American dust barrier also has implications for equatorial aquatic ecosystems located to the west of the Central American coastline. In this region, high phytoplankton growth inferred from chlorophyll concentration observations during July [Falkowski et al., 1998], suggest that the Central American dust barrier serves as a natural inhibitor of carbon sequestration in the Pacific. Additionally, transported dust distributions will be sensitive to variability in Saharan dust emissions, AEJ strength, and Inter-Tropical

Convergence Zone (ITCZ) position. Prospero and Lamb [2003] showed that dust transported from the Sahara to the Caribbean is linked to Sahel precipitation from the previous year. Another caveat is that we expect the Central American dust barrier to exist only in summer months. The AEJ forms during northern hemisphere summer and corresponds with peak dust transport from the Sahara to Caribbean. Offline analysis of the MODIS-Terra 2000 – 2010 monthly climatology suggests that transported dust loadings are too low to see evidence of a Central American dust barrier during non-summer months. One final caveat is that the strength of our results lies in the ability of our model to accurately simulate dust loss processes. In particular, our analysis relies heavily on the ability of the model to provide a realistic representation of convection, which subsequently influences wet removal over the Caribbean. Because wet removal rates are not typically measured in the field, it is difficult to determine whether our parameterization of wet removal is accurate and therefore we are limited to relying on proxies, such as column AOT. As previously discussed, our baseline simulation provided a weak representation of the Central American dust barrier when compared to MODIS-Terra, suggesting that our wet removal rates were too relaxed in the model (Figure 2). However, when compared to the GPCP observations, the July 2007 mean GEOS-5 precipitation was slightly greater over most of the Caribbean (Figure 8). These results suggest that the connection between wet removal and precipitation should be strengthened in GEOS-5, in particular that our simulation which best captured this dust barrier was the one that treated dust the same as hygroscopic aerosol species with respect to wet removal processes, suggesting that the best representation of dust in our model is one which allows that dust has mixed or been processed so as to be more hydrophilic.

Figure 1.

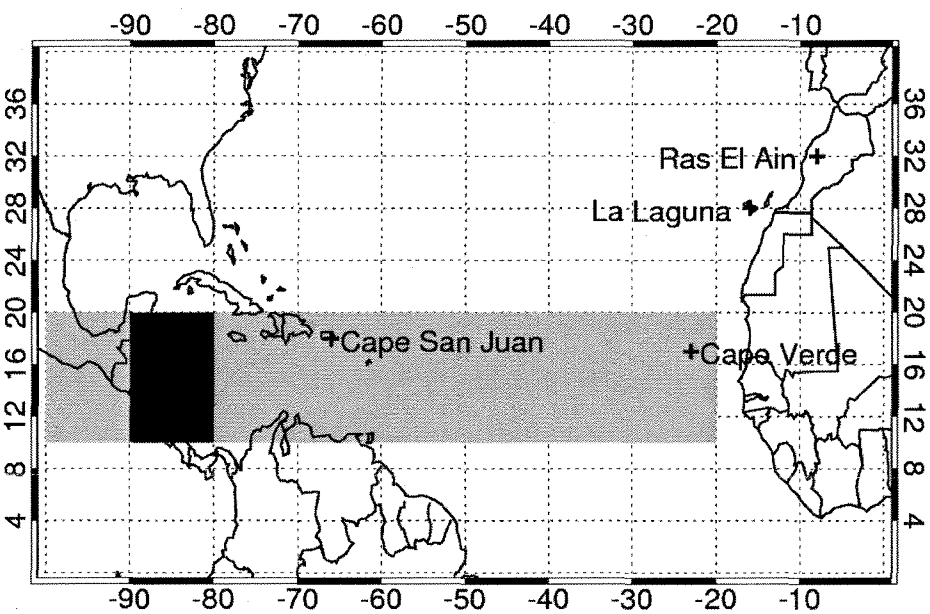

Figure 1. AERONET site locations and dust barrier-averaging regions (shaded).

Figure 2.

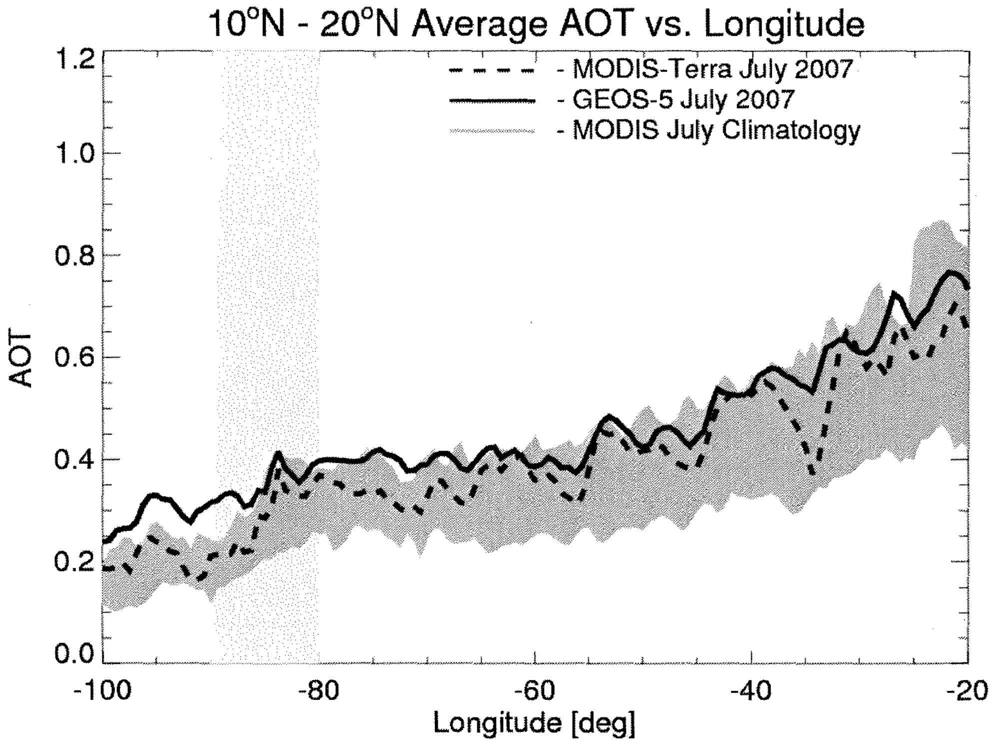

Figure 2. MODIS-Terra/Aqua July climatological (2002-2010) AOT (shading), MODIS-Terra July 2007 AOT (dashed) and GEOS-5 sampled (solid) July 2007 AOT averaged from 10°-20° N.

Figure 3.

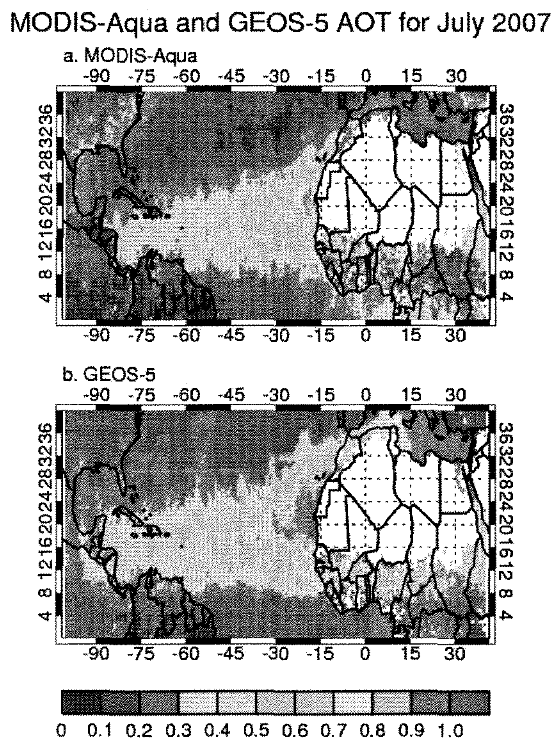

Figure 3. MODIS-Aqua (a) and GEOS-5 sampled (b) July 2007 AOT

Figure 4.

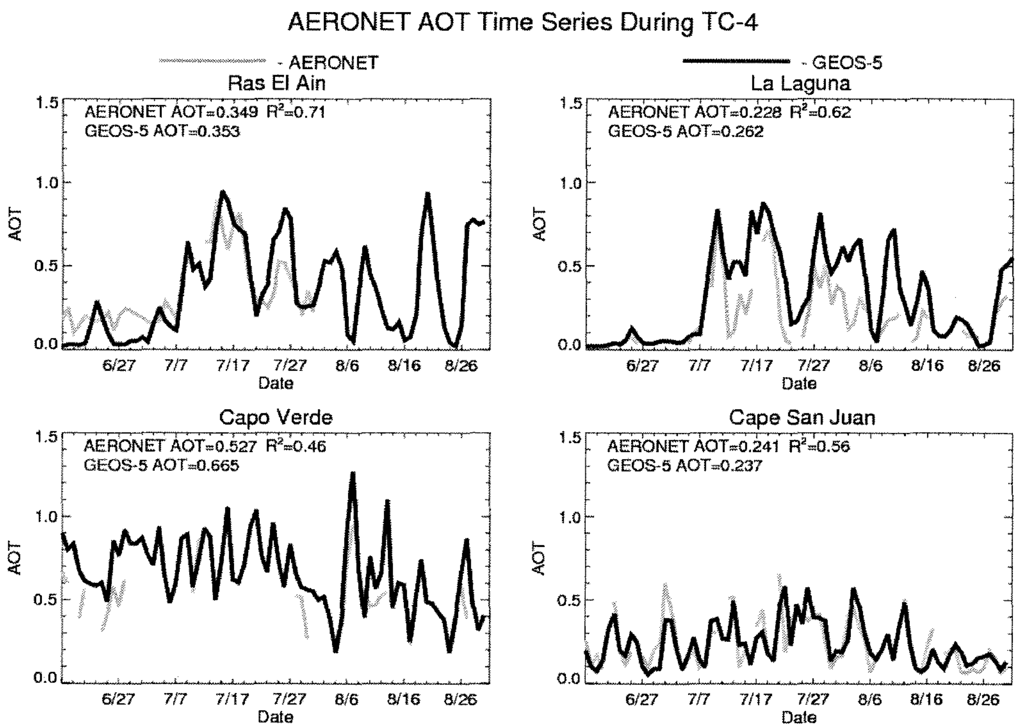

Figure 4. AERONET and GEOS-5 AOT time series.

Figure 5.

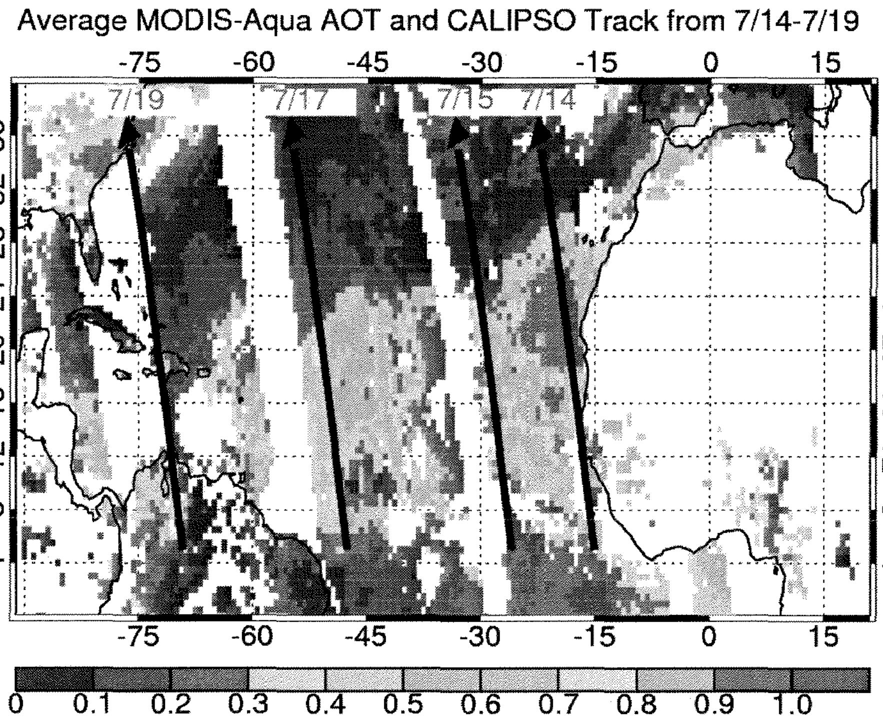

Figure 5. Average MODIS-Aqua AOT and CALIPSO track from 14-19 July.

Figure 6.

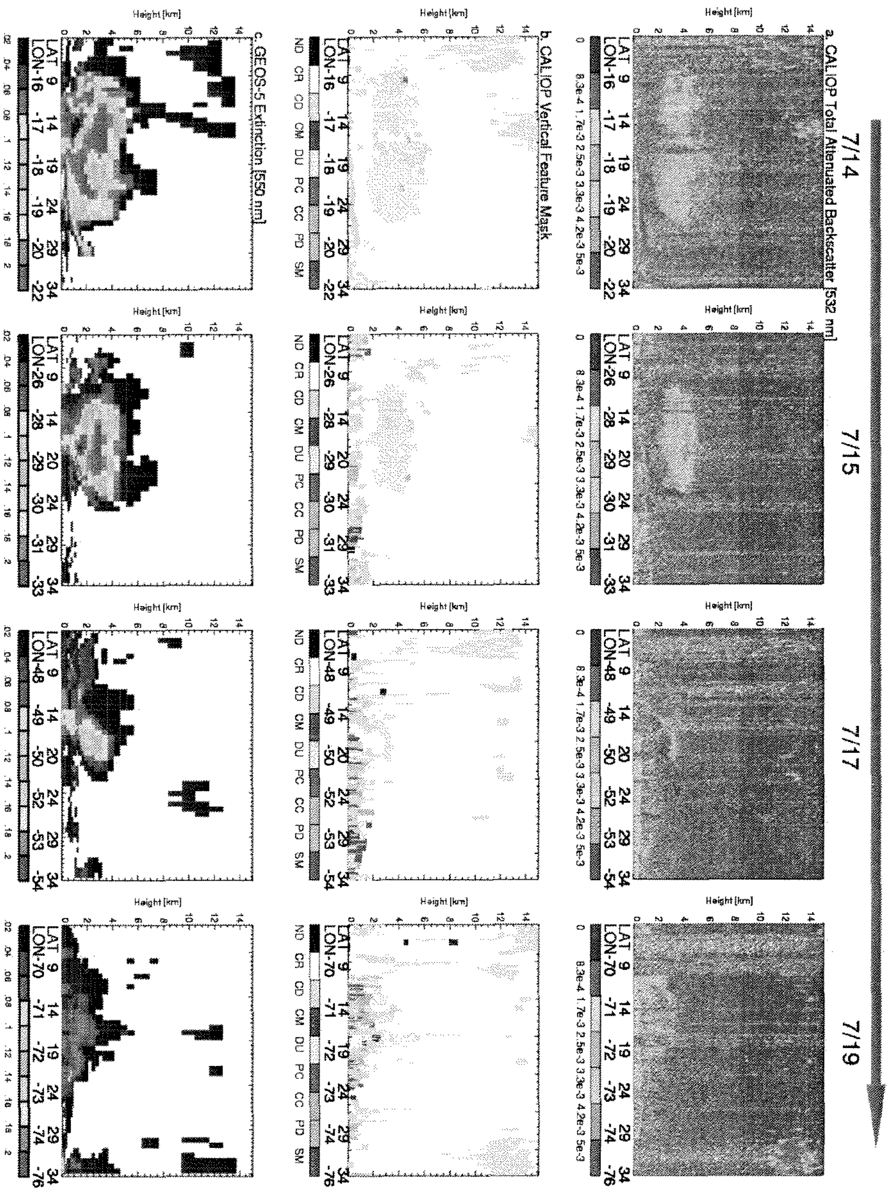

Figure 6. CALIOP total attenuated backscatter [km^{-1} sr^{-1}] (a), CALIOP vertical feature mask (b), and GEOS-5 extinction [km^{-1}] (c) for a dust event tracked from Africa (14 July) to the Caribbean (19 July).

Figure 7.

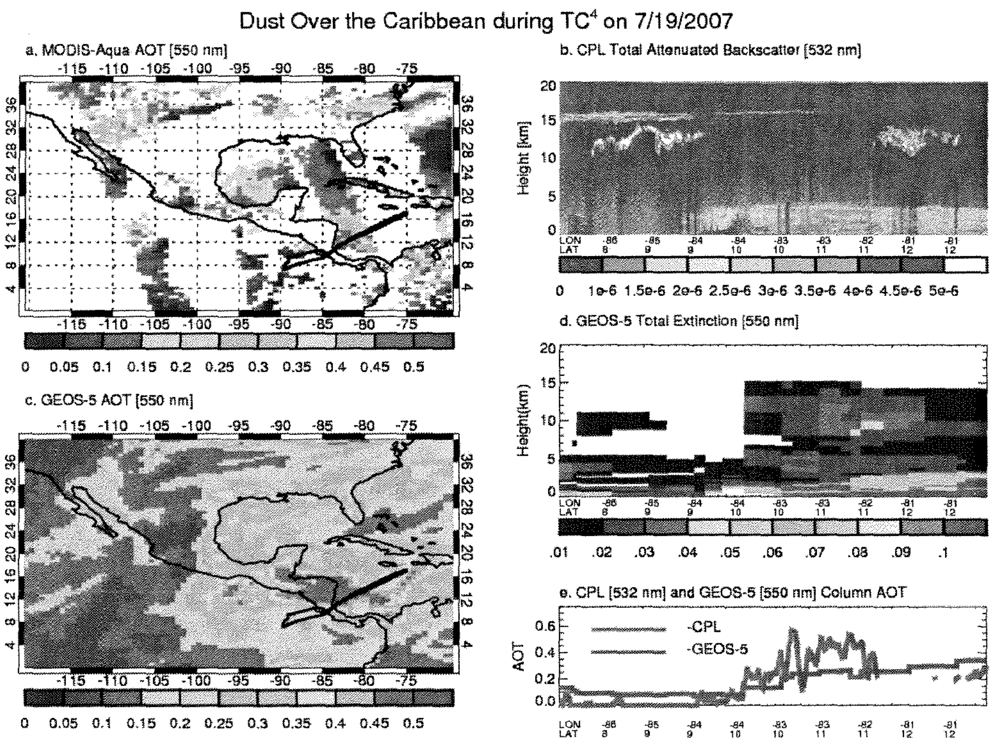

Figure 7. MODIS Aqua AOT (a), CPL total attenuated backscatter [km^{-1} sr^{-1}] (b), GEOS-5 AOT (c), GEOS-5 extinction [km^{-1}] (d), CPL AOT below 5 km (red) and GEOS-5 AOT below 5 km (blue) (e) on 19 July 2007.

Figure 8.

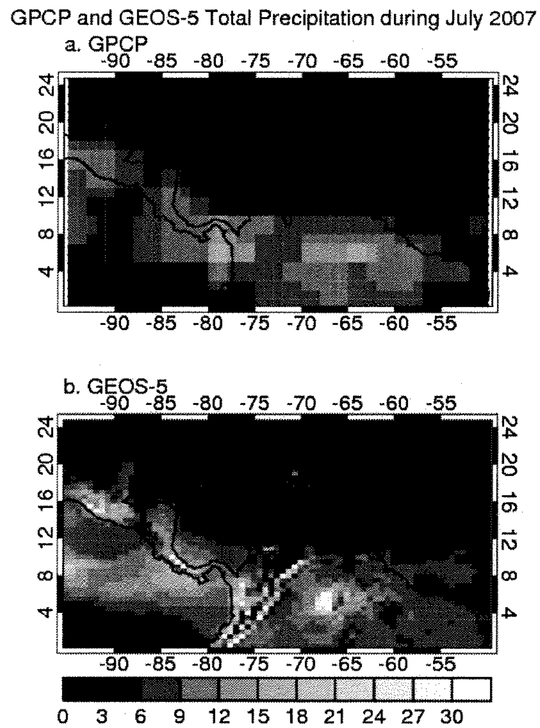

Figure 8. July 2007 monthly mean GPCP (a) and GEOS-5 (b) total precipitation [mm dy^{-1}].

Figure 9.

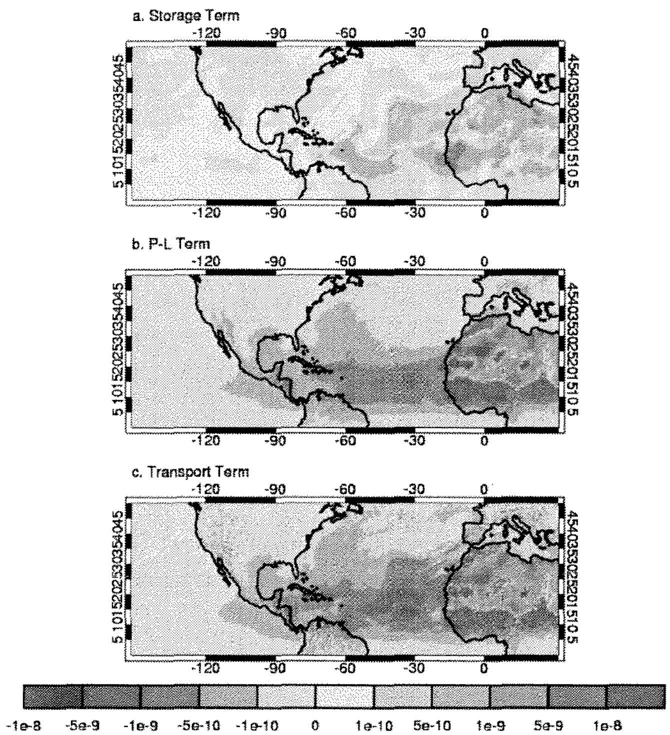

Figure 9. July 2007 storage(a) production minus loss (P – L) (b), and divergence terms (c) in kg m^{-2} s^{-1}.

Figure 10.

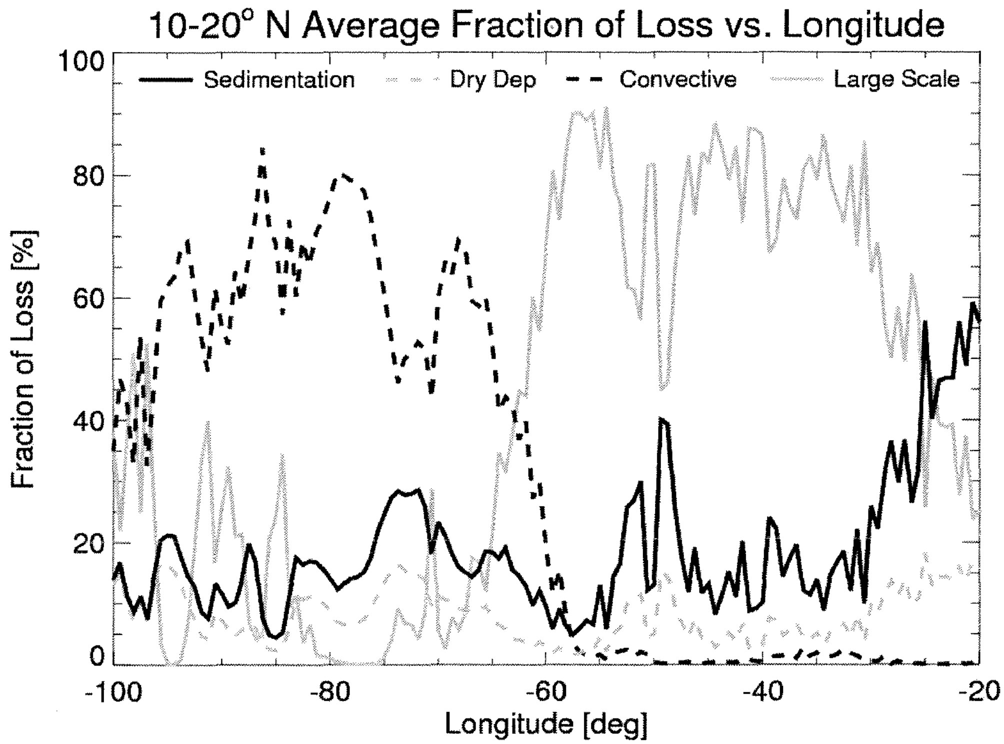

Figure 10. 10°-20° N July 2007 average significance of sedimentation, dry deposition, large scale scavenging, and convective scavenging.

Figure 11.

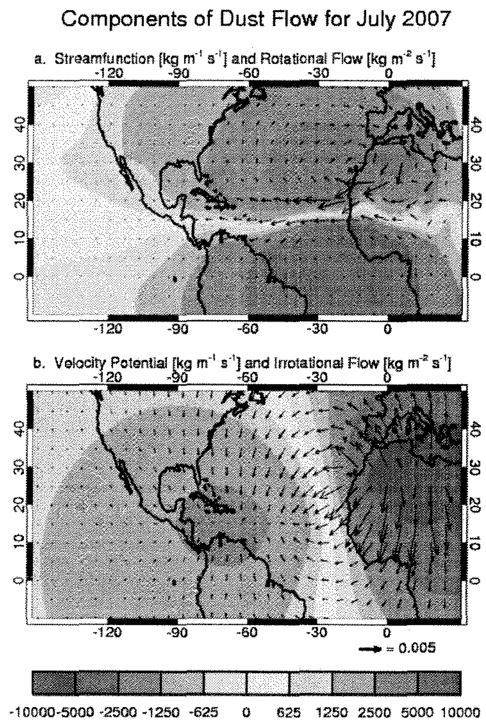

Figure 11. July 2007 mean streamfunction (a) and velocity potential (b). Rotational (top) and irrotational (bottom) flows are indicated by vectors.

Figure 12.

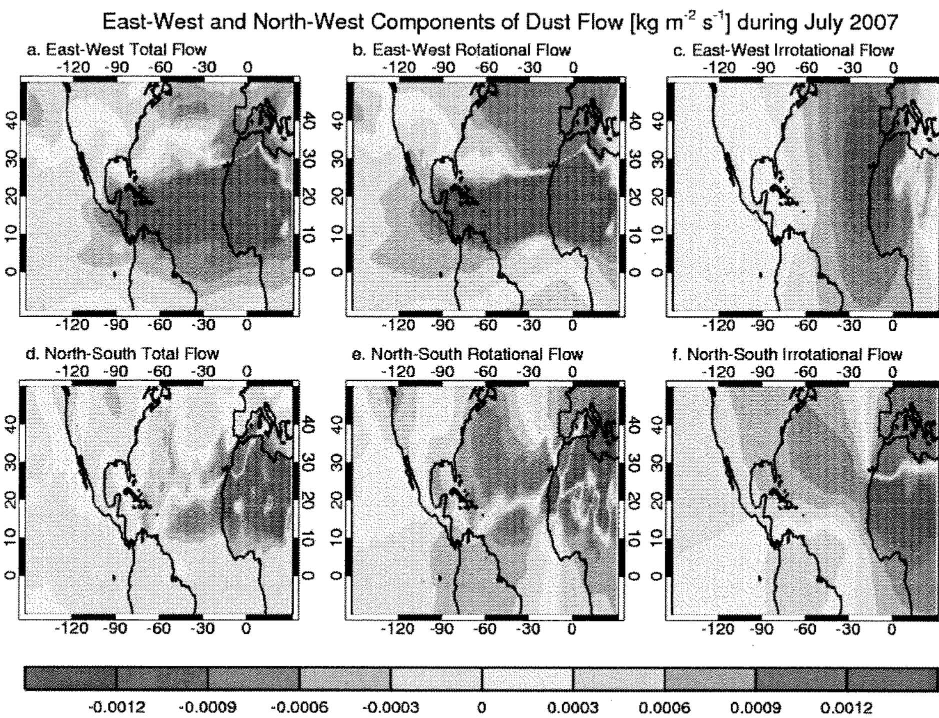

Figure 12. East-west (top) and north-south components (bottom) of the total (left), rotational (center), and divergent (right) flow.

Figure 13.

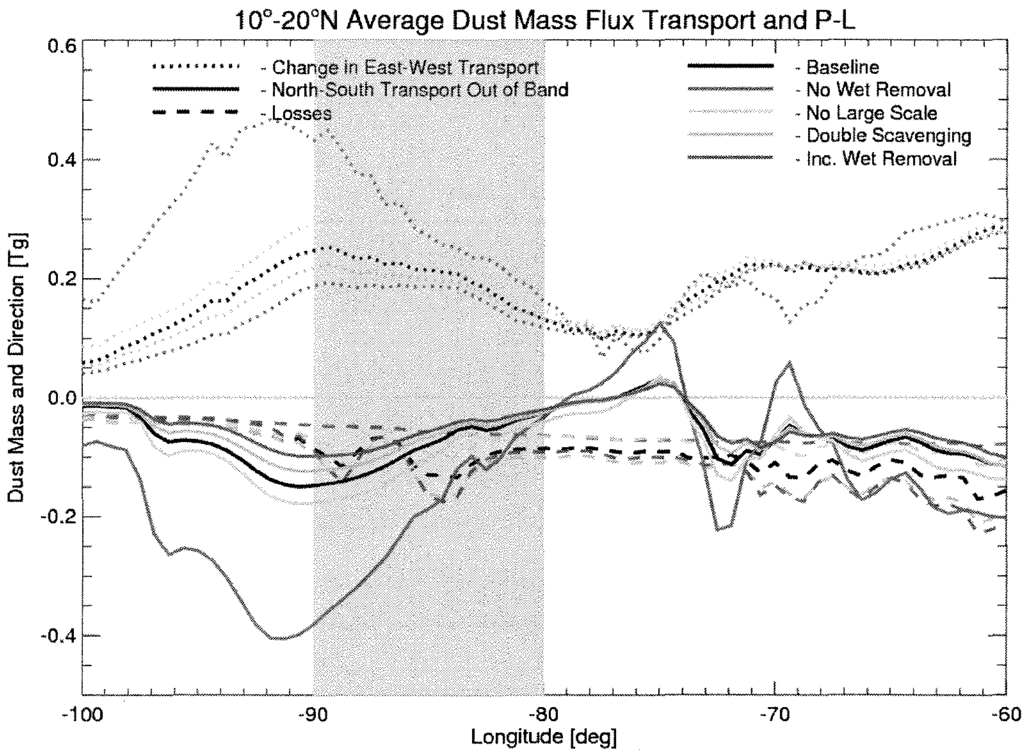

Figure 13. 10°-20° N July 2007 mass budget for our baseline, no wet removal, no large-scale scavenging, doubled scavenging, wet removal treated as other aerosols sensitivity tests. Shaded region indicates integration region for the Central American dust barrier.

Figure 14.

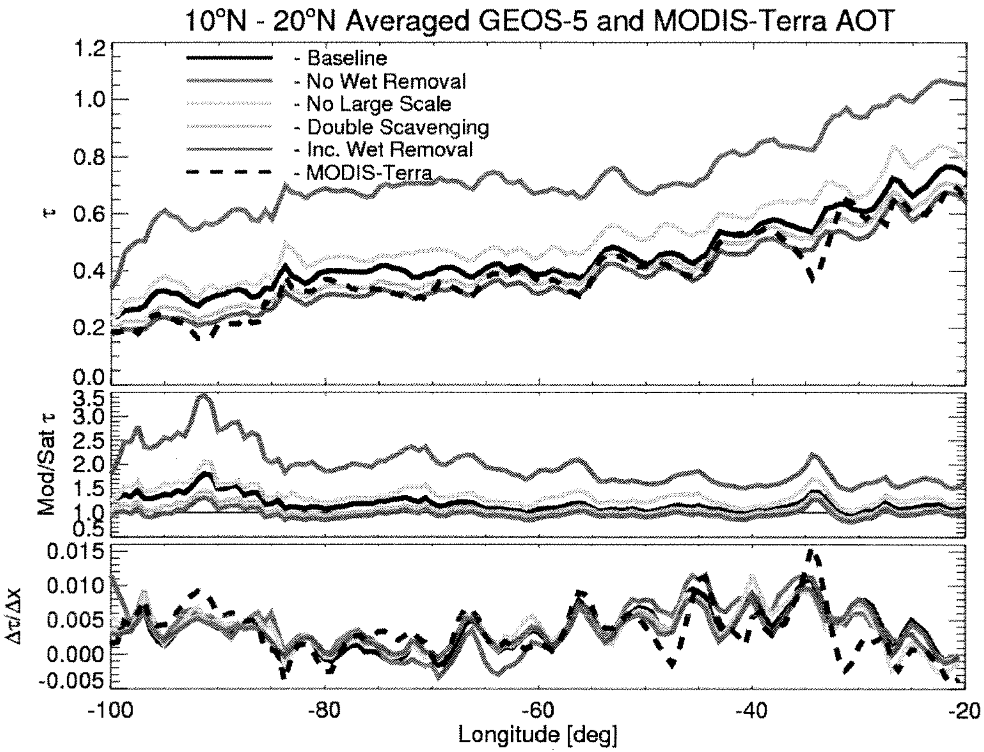

Figure 14. 10° N - 20° N averaged AOT, model to satellite AOT ratio, and AOT slope for MODIS-Terra and sampled baseline, no wet removal, no large-scale scavenging, doubled scavenging, and wet removal treated as other aerosols sensitivity tests. The thin black line indicates the one-to-one line for ratio plots.

Table 1

Experiment/Satellite	Net Northward Mass Transport (Tg) and Barrier Contribution (%)	Net Mass Loss from Removal (Tg) and Barrier Contribution (%)	80° W, 90° W, and Net Change in Westward Transport (Tg)	Barrier Efficiency		
				Mass	Total AOT	Coarse Mode AOT
1. Baseline	-1.46 | 47%	-1.67 | 53%	-7.58 | -4.21 | 3.37	0.36	0.21	0.17
2. Doubled Convective Scavenging	-1.24 | 39%	-1.90 | 61%	-6.51 | -3.40 | 3.11	0.48	0.25	0.21
3. Wet Removal Treated As Other Aerosols	-1.02 | 34%	-1.97 | 66%	-5.42 | -2.60 | 2.82	0.52	0.28	0.22
4. No Large Scale Scavenging	-1.85 | 59%	-0.95 | 41%	-9.76 | -6.88 | 3.87	0.33	0.19	0.16
5. No Wet Removal	-3.35 | 78%	-1.28 | 22%	-18.73 | -13.96 | 4.77	0.25	0.17	0.13
6. MODIS-Terra					0.37	0.30

Table 1. Net northward mass transport and mass loss from removal and relative contribution, westward mass transport at entrance and exit of barrier region, and mass, total AOT, and coarse mode barrier efficiencies for all simulations and MODIS-Terra.

Acknowledgements –

We would like to thank Brent Holben, Francisco Javier Exposito Gonzalez, Bernard Mougenot, Olivier Hagolle, Didier Tanre, and Olga Mayo-Bracero for their efforts in establishing and maintaining the Capo Verde, Ras El Ain, La Laguna, and Cape San Juan AERONET sites. Additionally, we would like to thank Judd Welton for his assistance with CALIOP data. This work was funded by the NASA Modeling, Analysis, and Prediction program and a NASA Earth System Science Fellowship.

References

Adler, R. F., Huffman, G. J., Chang, A., Ferraro, R., Xie, P.-P., Janowiak, J., Rudolf, B., Schneider, U., Curtis, S., Bolvin, D., Gruber, A., Susskind, J., Arkin, P., and Nelkin, E.: The Version-2 Global Precipitation Climatology Project (GPCP) Monthly Precipitation Analysis (1979–Present). J. Hydrometeor, 4, 1147–1167, 2003.

Brown, R. A.: Fluid Mechanics of the Atmosphere, Academic Press Inc., San Diego, CA, 1991.

Carlson, T. N., and Prospero, J. M.: The large-scale movement of Saharan air outbreaks over the northern equatorial Atlantic, J. Appl. Meteorol., 11, 283-297, 1972.

Chin, M., Ginoux, P., Kinne, S., Torres, O., Holben, B., N., Duncan, B. N., Martin, R. V., Logan, J. A., Higurashi, A., and Nakajima, T: Tropospheric aerosol optical thickness from the GOCART model and comparisons with satellite and sun photometer measurements, J. Atmos. Sci., 59(3), 461-483, 2002.

Colarco, P. R., Toon, O.B., Reid, J. S., Livingston, J. M., Russell, P. B., Redemann J., Schmid, B., Maring, H. B., Savoie, D., Welton, E. J., Campbell, J. R., Holben, B. N., and Levy, R.: Saharan dust transport to the Caribbean during PRIDE: 2. Transport, vertical profiles, and deposition in simulations of in situ and remote sensing observations, J. Geophys. Res., 108(D19), 8590, doi:10.1029/2002JD002659, 2003.

Colarco, P. R., da Silva, A., Chin, M., and Diehl, T.: Online simulations of global aerosol distributions in the NASA GEOS-4 model and comparisons to satellite and ground-based aerosol optical depth, J. Geophys. Res., 115, D14207, doi:10.1029/2009JD012820, 2010.

Cook, K. H.: Generation of the African Easterly jet and its role in determining West African precipitation. J. Climate, 12, 1165-1184, 1999.

DeMott, P. J., Sassen, K., Baumgardner, D., Rogers, D. C., Brooks, S. D., Prenni, A. J., and Kreidenweis, S. M.: African dust aerosols as atmospheric ice nuclei, Geophys. Res. Lett., 30(14), 1732, doi:10.1029/2003GL017410, 2003.

Desboeufs, K.V., Losno, R., and Colin, J.: Factors influencing aerosol solubility during cloud processes, Atmos. Environ., 35, 3529-3527, doi:10.1016/S1352-2310(00)00472-6, 2001.

Dubovik, O., and King, M. D.: A flexible inversion algorithm for retrieval of aerosol optical properties from sun and sky radiance measurements, J. Geophys. Res., 105(D16), 20673-20696, 2000.

Duce, R. A., and Tindale, N. W: Atmospheric transport of iron and its deposition in the ocean, Limnol. Oceanogr., 36, 1715–1726, 1991.

Dunion, J. P., and Velden, C. S.: The impact of the Saharan air layer on Atlantic tropical cyclone activity, Bull. Am. Meteorol. Soc., 85(3), 353 – 365, 2004.

Falkowski, P. G., Barber, R. T., and Smetacek, V.: Biogeochemical controls and feedbacks on primary production, Science, 281, 200-206, 1998.

Ginoux, P., Chin, M., Tegen, I., Prospero, J. M., Holben, B. N., Dubovik, O., and Lin, S.-J.: Sources and distributions of dust aerosols simulated with the GOCART model, J. Geophys. Res., 106(D17), 20255-20273, 2001.

Hand, J., Mahowald, N., Chen, Y., Siefert, R., Lou, C., Subramaniam, A., and Fung, I.:

Estimates of soluble iron from observations and a global mineral aerosol model: Biogeochemical implications, J. Geophys. Res., 109, D17205, doi:10.1029/2004JD004574, 2004.

Haywood, J., P. Francis, S. Osborne, M. Glew, N. Loeb, E. Highwood, D. Tanré, G. Myhre, P. Formenti, and E. Hirst (2003),

Haywood, J., Francis, P, Osborne, S., Glew, M., Loeb, N., Highwood, E., Tanré, D., Myhre, G., Formenti, P., and Hirst, E.: Radiative properties and direct radiative effect of Saharan dust measured by the C-130 aircraft during SHADE: 1. Solar spectrum, J. Geophys. Res., 108(D18), 8577, doi:10.1029/2002JD002687, 2003.

Hill, C., DeLuca, C., Balaji, V., Suarez, M., da Silva, A., and the ESMF Joint Specification Team: The Architecture of the Earth System Modeling Framework, Computing in Sci. and Eng., 6, 1-6, 2004.

Holben, B. N., Tanré, D., Smirnov, A., Eck, T. F., Slutsker, I., Abuhassan, N., Newcomb, W. W., Schafer, J. S., Chatenet, B., Lavenu, F., Kaufman, Y. J., Vande Castle, J., Setzer, A., Markham, B., Clark, D., Frouin, R., Halthore, R., Karneli, A., O'Neill, N. T., Pietras, C., Pinker, R. T., Voss, K., and Zibordi, G.: An emerging ground-based aerosol climatology: Aerosol optical depth from AERONET, J. Geophys. Res., 106(D11), 12067-12097, 2001.

Huffman, G. J., R. F. Adler, M. Morrissey, D. Bolvin, S.Curtis, R. Joyce, B. McGavock, and J.Susskind

Huffman, G. J., Adler, R. F., Morrissey, M., Bolvin, D., Curtis, S., Joyce, R., McGavock, B., and Susskin, J: Global Precipitation at One-Degree Daily Resolution from Multisatellite Observations. J. Hydrometeor, 2, 36–50, 2001.

Jickells, T. D., An, Z. S., Andersen, K. K., Baker, A. R., Bergametti, G., Brooks, N., Cao, J. J., Boyd, P. W., Duce, R. A., Hunter, K. A., Kawahata, H., Kubilay, N., LaRoche, J., Liss, P. S., Mahowald, N., Prospero, J. M., Rigwell, A. J., Tegen, I., and Torres, R.: Global iron connections between desert dust, ocean biogeochemistry, and climate, Science, 308(5718), 67-71, 2005.

Karyampudi, V. M., Palm, S. P., Reagan, J. A., Fang, H., Grant, W. B., Hoff, R. M., Moulin, C., Pierce, H. F., Torres, O., Browell, E. V., and Melfi, S. H.: Validation of the Saharan dust plume conceptual model using lidar, Meteosat, and ECMWF data, Bull. Am. Meteorol. Soc., 80, 1045-1075, 1999.

Kaufman, Y. J., Koren, I., Remer, L. A., Tanré, D., Ginoux, P., and Fan, S.:Dust transport and deposition observed from the Terra-Moderate Resolution Imaging Spectroradiometer (MODIS) spacecraft over the Atlantic Ocean, J. Geophys. Res., 110, D10S12, doi:10.1029/2003JD004436, 2005.

Kieber, R. J., Willey, J. D, and Avery, G. B.,: Temporal variability of rainwater iron speciation at the Bermuda Atlantic Time Series Station, J. Geophys. Res., 108(C8), 3277, doi:10.1029/2001JC001031, 2003.

Lau, W. K.M., and Kim, K.-M.: How Nature Foiled the 2006 Hurricane Forecasts, Eos Trans. AGU, 88(9), doi:10.1029/2007EO090002, 2007.

Levy, R. C., Remer, L.A., Kleidman, R. G., Mattoo, S., Ichoku, C., Kahn, R., and Eck, T. F.: Global evaluation of the Collection 5 MODIS dark-target aerosol products over land, Atmos. Chem. Phys., 10, 10399-10420, doi:10.5194/acp-10-10399-2010, 2010.

Mahowald, N. M., Baker, A. R., Bergametti, G., Brooks, N., Duce, R. A., Jickells, T. J., Kubilay, N., Prospero, J. M., and Tegen, I.: Atmospheric global dust cycle and iron inputs to the ocean, Global Biogeochem. Cycles, 19, GB4025, doi:10.1029/2004GB002402, 2005.

McGill, M. J., Hlavka, D. L., Hart, W. D., Scott, V. S., Spinhirne, J. D, , and Schmid, B.: The cloud physics lidar: Instrument description and initial measurement results, Appl. Opt., 41, 3725 – 3734, 2002.

McGill, M. J., Hlavka, D. L, Hart, W. D., Welton, E. J., and Campbell, J. R.: Airborne lidar measurements of aerosol optical properties during SAFARI-2000, J. Geophys. Res., 108(D13), 8493, doi:10.1029/2002JD002370, 2003.

McGill, M. J., Li, L., Hart, W. D., Heymsfield, G. M., Hlavka, D. L., P. E., Tian, L., Vaughan, M. A., and Winker, D. M.: Combined lidar-radar remote sensing: Initial results from CRYSTAL-FACE, J. Geophys. Res., 109, D07203, doi:10.1029/2003JD004030, 2004.

Nowottnick, E., Colarco, P., Ferrare, R., Chen, G., Ismail, S., Anderson, B., and Browell, E.: Online simulations of mineral dust aerosol distributions: Comparison to NAMMA observations and sensitivity to dust emission parameterization, J. Geophys. Res., 115, D03202, doi:10.1029/2009JD012692, 2010.

Pawson, S., Stolarski, R. S., Douglass, A. R., Newman, P. A., Nielsen, J. E., Frith, S. M., and Gupta, M. L.: Goddard Earth Observing System chemistry-climate model simulations of stratospheric ozone-temperature coupling between 1950 and 2005, J. Geophys. Res., 113, D12103, doi:10.1029/2007JD009511, 2008.

Petit, R. H., Legrand, M, Jankowiak, J., Molinié, J., Asselin de Beauville, C., Marion, G., and Mansot, J. L.: Transport of Saharan dust over the Caribbean Islands:

Study of an event, J. Geophys. Res., 110, D18S09, doi:10.1029/2004JD004748, 2005.

Pfister, L., Selkirk, H. B., Starr, D. O., Rosenlof, K., and Newman P. A.: A meteorological overview of the TC4 mission, J. Geophys. Res., 115, D00J12, doi:10.1029/2009JD013316, 2010.

Prospero, J. M., Ginoux, P., Torres, O., Nicholson, S. E., and Gill, T. E.: Environmental characterization of global sources of atmospheric soil dust identified with the Nimbus 7 Total Ozone Mapping Spectrometer (TOMS) absorbing aerosol product, Reviews of Geophysics, 40(1), 1002, doi:10.1029/2000RG000095, 2002.

Prospero, J., and Lamb, P.: African droughts and dust transport to the Caribbean: climate change implications, Science, 302, 1024 – 1027, 2003.

Remer, L. A., Kaufman, Y. J., Tanré, D., Mattoo, S., Chu, D. A., Martins, J. V., Li, R.-R., Ichoku, C., Levy, R. C., Kleidman, R. G., Eck, T. F., Vermote, E., and Holben, B. N.: The MODIS aerosol algorithm, products, and validation, J. Atmos. Sci., 62(4), 947-973, 2005.

Rienecker, M. M., Suarez, M. J., Todling, R., Bacmeister, J., Takacs, L., Liu, H.-C., Gu, W., Sienkiewicz, M., Koster, R. D., Gelaro, R., Stajner, I., and Nielsen, J. E.: The GEOS- 5 Data Assimilation System -Documentation of Versions 5.0.1, 5.1.0, and 5.2.0. Technical Report Series on Global Modeling and Data Assimilation 104606, 27, 2008.

Rienecker, M., et al., MERRA – NASA's Modern-Era Retrospective Analysis for Research and Applications. J. Climate, Submitted, 2011.

Rosenfeld, D., Rudich, Y., and Lahav, R.: Desert dust suppressing precipication: A possible desertification loop, Proceedings of the National Academy of Sciences, 98(11), 5975-5980, 2001.

Smirnov, A, Holben, B. N., Eck, T. F., Dubovik, O., and Slutsker, I.: Cloud-screening and quality control algorithms for the AERONET database, Remote Sens. Environ., 73(3), 337-349, 2000.

Sokolik, I. N., and Toon, O. B.: Direct radiative forcing by anthropogenic airborne mineral aerosols, Nature, 381(6584), 681-683, 1996.

Toon, O. B., Starr, D. O., Jensen, E. J., Newman, P. A., Platnick, S., Schoeberl, M. R., Wennberg, P. O., Wofsy, S. C., Kurylo, M. J., Maring, H., Jucks, K. W., Craig, M. S., Vasques, M. F., Pfister, L., Rosenlof, K. H., Selkirk, H. B., Colarco, P. R., Kawa, S. R., Mace, G. G., Minnis, P., and Pickering, K. E.: Planning, implementation, and first results of the Tropical Composition, Cloud and Climate Coupling Experiment (TC4), J. Geophys. Res., 115, D00J04, doi:10.1029/2009JD013073, 2010.

Vaughan, M. A. , Young, S., Winker, D., Powell, K., Omar, A., Liu, Z., Hu, Y., and Hostetler, C.: Fully automated analysis of space-based lidar data: An overview of the CALIPSO retrieval algorithms and data products, Proc. SPIE Int. Soc. Opt. Eng., 5575, 16-30, 2005.

Zhu, X. R., Prospero, J. M., and Millero, F. J.: Diel variability of soluble Fe(II) and soluble total Fe in North African dust in the trade winds at Barbados, J. Geophys. Res., 102(D17), 21,297–21,305, doi:10.1029/97JD01313, 1997.

Zhu, A., Ramanathan, V., Li, F., and Kim, D.: Dust plumes over the Pacific, Indian, and Atlantic oceans: Climatology and radiative impact, J. Geophys. Res., 112(D16), D16208, doi:10.1029/2007JD008427, 2007.